



Research article

Single-nucleus transcriptome unveils the role of ferroptosis in ischemic stroke

Cheng-Long Shi^a, Xiu-Li Han^b, Jing-Ce Chen^c, Qian-Fan Pan^a, Yong-Chao Gao^a, Peng-Yan Guo^a, Xiao-Li Min^{a,**}, Yong-Jun Gao^{a,*}

^a Department of Neurosurgery, The Second Affiliated Hospital of Kunming Medical University, Kunming, 650032, China

^b Department of Stomatology, Kunming Children's Hospital, Kunming, 650100, China

^c Department of Orthopedics, The First People's Hospital of Yunnan Province, Kunming, 650100, China

ARTICLE INFO

Keywords:

Stroke
snRNA-seq
Ferroptosis
Microglia

ABSTRACT

Multiple cell death pathways are involved in neuronal death in ischemic stroke (IS). However, the role of different cell death pathways in different cell types has not been elucidated. By analyzing three single-nucleus RNA sequencing (snRNA-seq) data of IS, we first found that a variety of programmed cell death (PCD)-related genes were significantly changed in different cell types. Based on machine learning and virtual gene knockout, we found that ferroptosis related genes, ferritin heavy chain 1 (Fth1) and ferritin light chain (Ftl1), play a key role in IS. Ftl1 and Fth1 can promote microglia activation, as well as the production of inflammatory factors and chemokines. Cell communication analysis showed that activated microglia could enhance chemotactic peripheral leukocyte infiltration, such as macrophages and neutrophils, through Spp1-Cd44 and App-Cd74 signaling, thereby aggravating brain tissue damage. Furthermore, real-time quantitative polymerase chain reaction (RT-qPCR) showed that P2ry12 and Mef2c were significantly decreased in oxygen-glucose deprivation (OGD) group, while Ftl1, Fth1, Apoe, Ctsb, Cd44 and Cd74 were significantly increased in OGD group. Collectively, our findings suggested targeted therapy against microglia Ftl1 and Fth1 might improve the state of microglia, reduce the infiltration of peripheral immune cells and tissue inflammation, and then improve the ischemic brain injury in mouse.

1. Introduction

Ischemic stroke (IS) is a common neurological disease, which is a pathological process of brain tissue hypoxia and energy metabolism disorder due to the reduction or interruption of cerebral blood flow, leading to cell damage and death [1,2]. IS represents one of the leading causes of death and disability worldwide and is common in both developed and developing countries [3], especially in the elderly group [2]. For acute IS, ongoing trials assess the effectiveness of thrombolytic, anti-inflammatory therapy, and neuroprotective approaches. Pharmacological and stem cell therapies are also expected to promote brain regeneration, rehabilitation, and functional recovery [4]. Despite the decline in stroke mortality, the global burden of stroke is increasing. Therefore, it is necessary to further study the mechanism of IS and related pathological processes, so as to provide a better theoretical basis for early intervention and treatment

* Corresponding author. No.374 Dianmian Road, Wuhua District, Kunming, 650032, Yunnan, China.

** Corresponding author. No.374 Dianmian Road, Wuhua District, Kunming, 650032, Yunnan, China.

E-mail addresses: minxiaoli@kmmu.edu.cn (X.-L. Min), gaoyongjun@kmmu.edu.cn (Y.-J. Gao).

<https://doi.org/10.1016/j.heliyon.2024.e32727>

Received 17 March 2024; Received in revised form 6 June 2024; Accepted 7 June 2024

Available online 14 June 2024

2405-8440/© 2024 Published by Elsevier Ltd. This is an open access article under the CC BY-NC-ND license (<http://creativecommons.org/licenses/by-nc-nd/4.0/>).

of IS.

At present, it is believed that neuronal death in ischemic stroke involves a variety of cell death pathways, including endogenous and exogenous apoptosis, necroptosis, autophagy, ferroptosis, PARP-1-dependent cell death and pyroptosis [5]. In IS, ferroptosis is considered to be an important factor leading to neuronal death and neurological dysfunction. Clinical studies have shown that iron levels are significantly increased in multiple regions of the brain in children with severe ischemia-hypoxic injury [6]. Ferroptosis is an iron-dependent form of regulated cell death in which the production and accumulation of lipid peroxides mediated by oxidative stress leads to cell death with rupture of cytoplasmic membranes accompanied by extensive tissue damage [7]. Ferroptosis is accompanied by lipid peroxidation and harmful free radical production, leading to neuronal and other brain cell damage and death [8–10]. Studies have shown that both ferrostatin-1 and liproxtinin-1 can significantly reduce the infarct volume and improve neurological deficits in middle cerebral artery occlusion (MCAO) mouse models [11]. In neurons, glutathione peroxidase 4 (GPX4) inhibits excessive lipid peroxidation, and inhibition of GPX4 activity triggers ferroptosis [12,13]. Further studies showed that specific induction of GPX4 knockdown triggers ferroptosis in motor neurons, and that inclusion of the lipid-based antioxidant vitamin E in the diet partially delayed this process [14]. Tat-SelPep, a seleno-containing peptide, can significantly reduce cerebral infarct size by driving GPX4 expression to inhibit ferroptosis [9]. Carvacrol, a natural monoterpene, protects hippocampal neurons from I/R injury in gerbils by increasing GPX4 expression [15]. These results suggest that ferroptosis plays an important role in cerebral ischemic injury. Although some progress has been made in the study of the mechanism of iron death, the study of iron death caused by IS remains still in its infancy. We need further research and experiments to gain a deeper understanding of this process and to develop effective interventions method.

In Ischemic stroke and ischemia-reperfusion injury, a large number of studies have shown the effect of iron death on neurons, but there are few studies investigating on microglia. Microglia are also susceptible to ferroptosis. Previous studies have shown that neurons that undergo iron death release patterns of injury-related molecules that can rapidly activate and recruit microglia, inducing the upregulation of NADPH oxidase and reactive oxygen species (ROS) production [16]. ROS can act as pro-inflammatory signaling molecules and promote the activation of microglia [17]. In addition, overactivated microglia secrete pro-inflammatory cytokines and chemokines, attract astrocytes and peripheral white blood cells, and exacerbate neuroinflammation and oxidative stress [18]. Finally, a vicious cycle of mutual promotion and self-amplification between oxidative stress, neuronal iron death and inflammatory response is formed, which is harmful to nerve survival [19]. However, microglia are also susceptible to iron death in other neurological diseases, and microglia have the greatest transcriptional response to iron overload and the greatest iron chelation capacity in co-culture systems compared to astrocytes and neurons [20]. Microglial iron overload and iron dysregulation lead to increased production and release of microglial cytokines, aggravating the pathological environment of the disease [21]. Recent studies have shown that BV2 cells and macrophages exhibit iron death resistance while undergoing severe inflammatory responses stimulated by LPS [22]. Previous studies have reported that the use of antioxidants to reduce oxidative stress, iron death inhibitors to inhibit iron death, and anti-inflammatory drugs to reduce neuroinflammation can all alleviate reperfusion injury to some extent [23,24].

In this study, to investigate the potential role of microglia ferroptosis in IS, we analyzed three snRNA-seq data and found that elevated ferroptosis related genes *Ftl1* and *Fth1* can promote microglia activation, thereby worsening cerebral ischemic injury.

2. Materials and methods

2.1. Data download and collection

By searching literature and databases, we collected snRNA-seq data from three cohort studies: GSE167593, GSE1997731, and GSE174574. Details of the sample, including database, sample ID, age, gender, can be found in the [Supplementary Table 1](#).

2.2. Pre-processing and quality control of snRNA-seq data

Cell Ranger 7.0.1 (10x Genomics) was used to process the raw sequencing data [25]. To further ensure the quality of our dataset, we only retained cells with the number of detected genes greater than 200 and the percentage of detected mitochondrial genes less than 10%. Doublets were detected using DoubletFinder (v2.0.3). After sample integration and clustering, clusters lacking specific marker genes, with relatively low gene content and high mitochondrial ratios were discarded.

2.3. Data integration

Data from different datasets were integrated separately. Briefly, unique molecular identifiers (UMIs) from each valid cell barcode were retained for all downstream analyses and analyzed using the R package Seurat (v4.2.2) [25,26]. After filtering, data from different sample underwent normalization (using “NormalizeData function with parameters “normalization.method = “LogNormalize”, scale.factor = 10000”) and identification of highly variable genes (HVGs) (using “FindVariableFeatures” function with the options “selection.method = “vst”, nfeatures = 3000”) [27]. Then, we applied “FindIntegrationAnchors” and “IntegrateData” functions to integrate all the sequencing libraries with the top 30 significant principal components (PCs) (dim = 1:30) [27]. The top 3000 HVGs of each dataset were used for downstream principal component analysis (PCA). The top 30 significant PCs were selected for clustering and visualization using uniform manifold approximation and projection (UMAP).

2.4. Identification of cell type specific marker genes

“FindMarkers” function implemented in Seurat v4.2.2 [28] was used to identify cell type specific marker genes with the options “logfc.threshold = 0.25, min.pct = 0.25”. P-value was corrected using the Bonferroni method, and 0.05 was set as a threshold to define significance.

2.5. Gene set score analysis

Gene set scores were acquired by analyzing the transcriptome of each input cell against aforementioned gene sets by the Seurat function “AddModuleScore”. In short, the expression mean of all genes was calculated, and bin was divided according to the expression mean to view the distribution of target genes in bin. 100 genes were randomly selected as background genes. Then, the average expression levels of each cell type were calculated on single cell level, subtracted by the average expression of control gene sets. Changes in the scores between group were analyzed using ggpubr function “compare_means” with the Wilcoxon test. Heat map visualization using the pheatmap function. ***(adjust P value) < 0.001, **(adjust P value) < 0.01, *(adjust P value) < 0.05.

2.6. Identification of differentially expressed genes (DEGs)

To identify genes differentially expressed between sham and MCAO, P values were calculated and FDR-corrected using MAST [29]. All nuclei from different group samples for corresponding cell types were used. MAST was used to perform zero-inflated regression analysis by fitting a linear mixed model. To exclude gene expression changes stemming from confounders, such as age, sex, fractions of ribosomal and mitochondrial transcripts, the following model for aging and sex was fit with MAST:

```
zlm (~condition + nCount_RNA + percent.mt, sca, method = glmer, ebayes = T)
```

Where percent.mt is mitochondrial RNA fraction.

Genes with at least 25 % increase or decrease in expression in a group versus other group and an false discovery rates (FDR)-corrected $P < 0.05$ were selected as differentially expressed.

2.7. Cell state prediction using machine learning

The snRNA-seq data were selected for Sham or MCAO classification. For each cell, one categorical feature (Group) and amount of gene expression features were used for machine learning. The pipeline and functions were implemented in automated machine learning R package h2o (v3.44.0.2). For data splitting, 25 % of nuclei were first split into the testing set, and the rest 75 % were further split into training and validation sets using 10 folds cross-validation and 20 max models. The best model is extracted using the function “h2o.get_best_model”. The function “h2o.predict” is used for the test and validation sets. Use the function “h2o.permutation_importance_plot” to obtain variable importance based on permutation.

2.8. Virtual knockout of the gene of interest

To elucidate the effect of specific gene knockout (KO) on group cell type function, we extract the snRNA-seq data of group-specific cell type and used the expression matrix of genes \times cells as the input for scTenifoldKnk analysis [30]. In the scTenifoldKnk analysis, the gene regulatory network (GRN) is first constructed using the snRNA-seq data, and then the target gene is deleted from the constructed GRN. Manifold alignment is used to align the resulting reduced GRN with the original GRN to identify difference-regulating genes that are used to infer the function of the target gene in the analysis cell. The virtual KO perturbed genes with FDR-corrected $P < 0.05$ were selected as differentially expressed. The interaction enrichment analysis was provided and based on the STRING protein-protein interaction database. The R package Enrichr (v3.2) was used for functional enrichment analysis.

2.9. BV2 cell culture

The BV2 cell lines in our laboratory were purchased from Qingqi Biotechnology Development Co., Ltd. (Shanghai, China). The cell line were cultured in high glucose medium containing 10 % inactivated fetal bovine serum in an incubator with 5 % CO₂ at 37 °C. When the cells reached 80 %–90 % confluence and grew well, they were digested with trypsin and subcultured.

2.10. Oxygen–glucose deprivation model construction

Cultured BV2 were firstly washed with PBS for three times and then placed into the glucose-free medium (Gibco) at 37 °C. Subsequently, the cells were transferred into a hypoxia chamber with the inner concentration of 95 % N₂, and 5 % CO₂ at 37 °C for 2 h. Afterwards, these obtained cells were put back into normal DMEM medium with 95 % air and 5 % CO₂, and incubated for 24 h for reoxygenation.

2.11. Real-time quantitative polymerase chain reaction (RT-qPCR)

The total RNA fraction was extracted using Trizol reagent (Takara, 9109, Japan) and reverse transcribed using RevertAid™ First

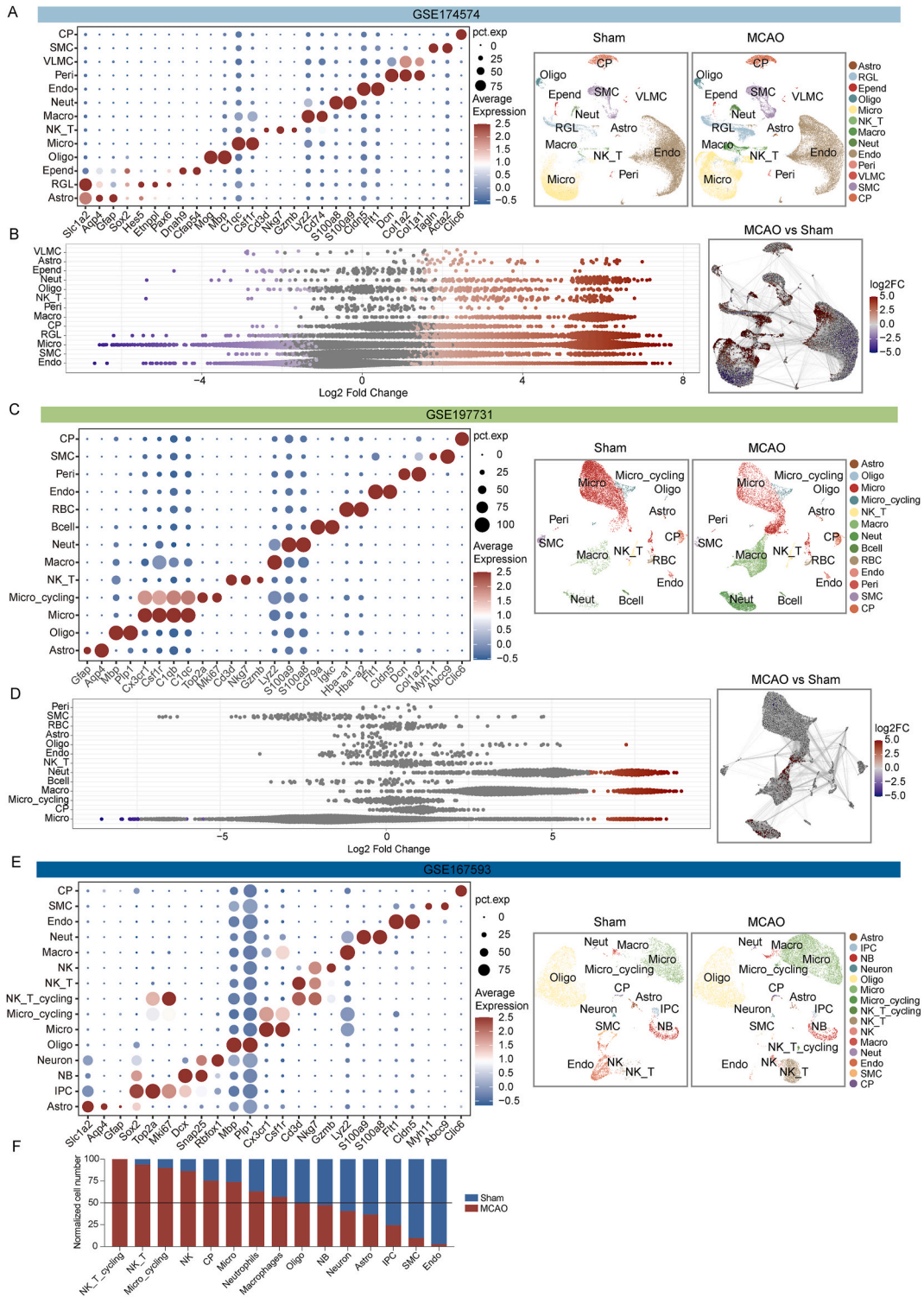


Fig. 1. Transcriptome profiling of mouse IS. A. Dot plot (left) shows cell type marker genes for the GSE174574 dataset. UMAP visualization (right) of different cell types in sham and MCAO groups. B. Scatter plots (left) and UMAP (right) demonstrate the difference in cell numbers between MCAO and Sham groups. C. Dot plot (left) shows cell type marker genes for the GSE197731 dataset. UMAP visualization (right) of different cell types in sham and MCAO groups. D. Scatter plots (left) and UMAP (right) demonstrate the difference in cell numbers between MCAO and Sham groups. E. Dot plot (left) shows cell type marker genes for the GSE167593 dataset. UMAP visualization (right) of different cell types in Sham and MCAO groups. F. Bar graphs show the proportion of different cell types in Sham and MCAO.

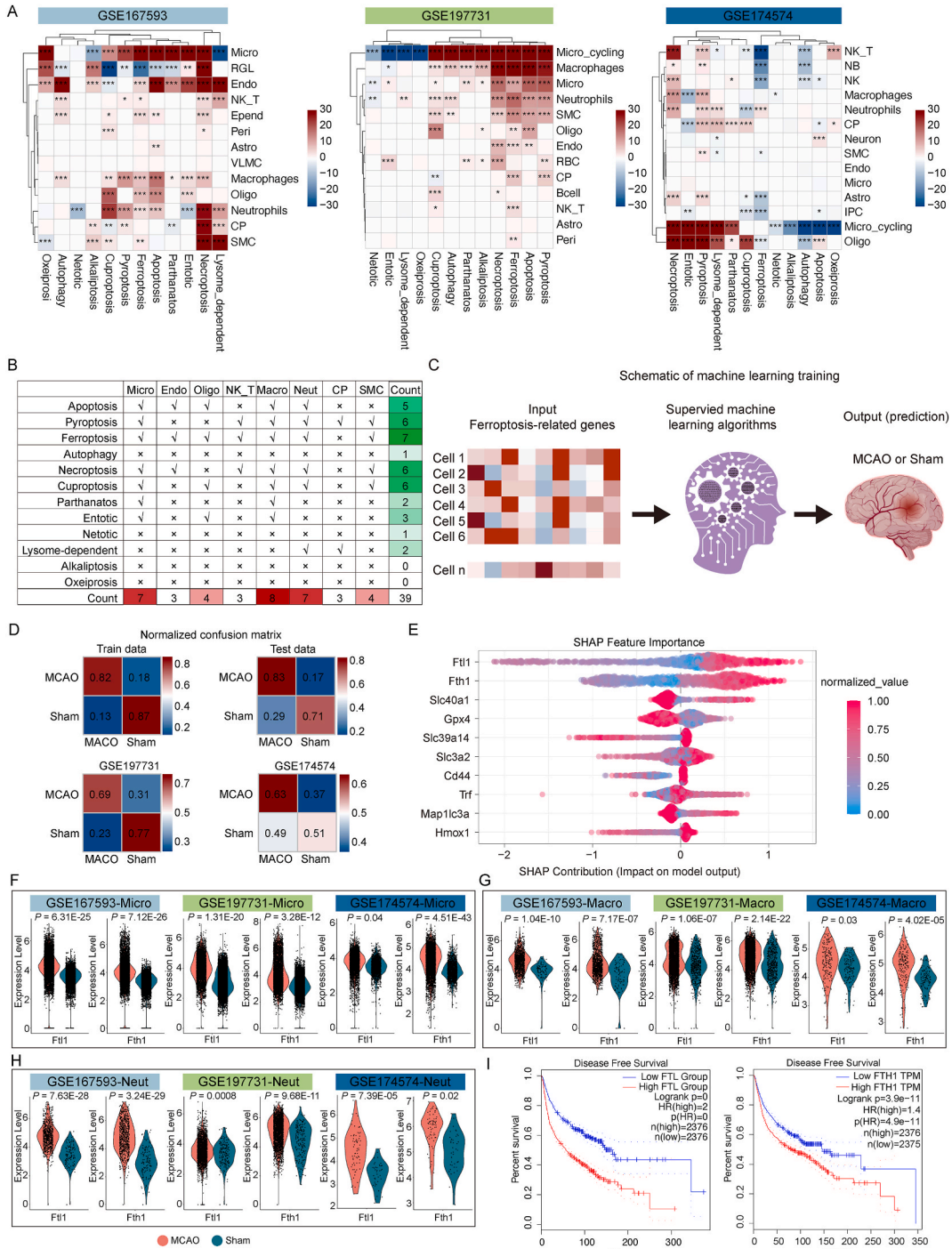


Fig. 2. PCD changed differentially between Sham and MCAO. **A.** Expression differences of programmed cell death (PCD)-related genes between Sham and MCAO group. **B.** PCD with consistent changes in at least two datasets. **C.** Schematic of the machine learning approach. **D.** Ferroptosis-related genes predict cell status. Confusion matrix depicting the model accuracy (left). **E.** Top 10 most important features of the model. **F.** Violin plot shows the expression of Ftl1 and Fth1 in microglia in Sham and MCAO groups. **G.** Violin plot shows the expression of Ftl1 and Fth1 in macrophages in Sham and MCAO groups. **H.** Violin plot shows the expression of Ftl1 and Fth1 in neutrophils in Sham and MCAO groups. **I.** Disease-free survival analysis of Ftl1 and Fth1.

Strand cDNA Synthesis System (Invitrogen). Quantitative PCR reactions were carried out with SYBR (DBI Bioscience). The expression level of each gene was normalized to that of β -actin using the $2^{-\Delta\Delta ct}$ method. Primers used for the reactions are as follows.

Gene	Forward	Reverse
β -actin	GAAGATCAAGATCATTGCTCCTC	ATCCACATCTGCTGGAAGG
P2ry12	CAGAAATCAACAGTTATCAGGTAACC	ACAGACTGGTGTACCAGG
Mef2c	GAACGTAACAGACAGGTGAC	CGCAATCTCACAGTCACAC
Ftl1	GAGAAGAACCTGAATCAGGC	CAGGAAGTCACAGAGATGAG
Fth1	GGATATAAAGAAACCAGACCGT	CTGTTCACCTCAGATAATACGTCTC
Apoe	GTTGCTGGTCACATTCTCG	TCATGGTCTCGTCCATCAG
Ctsb	GACATGAGTACTTGAAGAGG	GTCCCTCGTAAACATAACTCTC
Cd74	CTTCCGAAATCTGCCAAACC	CATGTTATCCATGGACATTGGAC
Cd44	GTACCTTACCACCATGGAC	TTCTTCTATGAACCCATACCTG

2.12. Acquisition of immunohistochemical data

To validate our results, we searched for protein expression of interest on database THE HUMAN PROTEIN ATLAS (<https://www.proteinatlas.org/>). The database provides more than 21,000 primary antibodies against the human protein profile. There are over 700 IHC, IF, WB result graphs for each antibody. All antibodies have undergone rigorous validation for specificity, reproducibility and product functionality and have been tested in a variety of experimental applications.

2.13. Statistical and reproducibility

If not specified, all statistical analyses and data visualization were done in R (v4.2.2). We state that no statistical method was used to predetermine sample size. No data were excluded from the analyses and the experiments were not randomized. RT-qPCR data were tested by two-tailed Student's t-test, followed by post hoc Tukey-Kramer test through SPSS 27.0 or GraphPad Prism v9.0. The error bars denote the mean \pm SEM. Normal distributions were tested by F-test.

3. Results

3.1. Construction of cell maps after IS in mouse

To investigate cellular changes following IS in mouse, we analyzed three publicly available snRNA-seq datasets of IS in mouse [31–33] (Fig. 1; Supplementary Table 1). All three data sets included sham group and MCAO model group (Supplementary Table 1). After rigorous data quality control and filtering, we obtained 66,056, 25,246, and 19,114 nuclei, as well as identified 13, 13, and 15 cell types, respectively (Fig. 1A–C, and E). Among them, microglia, macrophages, neutrophils, proliferative microglia, NK and T cells accounted for a large proportion in the three data sets, while the number of neurons was small or even absent. Since changes in the proportions of one cell type can potentially distort changes in other cell types, we then applied the differential abundance testing algorithm (Milo) [34] to identify cells that changed significantly after IS (Fig. 1B–D). The results showed that microglia, macrophages, and neutrophils were significantly increased in MCAO (Fig. 1B–D). Analysis of the normalized cell numbers from the GSE174574 data set yielded similar results (Fig. 1F).

3.2. Multiple modes of cell death are involved in cerebral ischemic injury in mouse

To investigate the role of different modes of cell death in cerebral ischemic injury, we evaluated the expression changes of 12 PCD-related genes [35] in different cell types after cerebral ischemic injury (Fig. 2A; Supplementary Table 2). By analyzing PCD with significant changes in at least two datasets, we found that microglia, macrophages, and neutrophils were involved in the most PCD (Fig. 2B). Among the 12 PCD types, ferroptosis was the most frequently involved cell type (Fig. 2B).

To this end, we tested whether ferroptosis-related genes could be used to predict the state of cells (Sham or MCAO) in the dataset (Fig. 2C). We applied an automated machine learning model (autoML), h2o, to classify cells as Sham or MCAO (Fig. 2C). Then, we selected the best classifier for model interpretation (Fig. 2D). The confusion matrices from the training set (GSE167393), test set (GSE167393), and two validation sets (GSE197731 and GSE174574) determined the performance of the model (Fig. 2D), that is, ferroptosis-related genes could accurately predict the state of cells (Fig. 2D). Then, to test the importance of each feature in the ferroptosis-related gene set, we performed a permutation-based importance analysis (Fig. 2E). The results showed that Ftl1 and Fth1 had the greatest impact on the performance of the model. In addition, the violin plot showed that the expression of Ftl1 and Fth1 was significantly higher in microglia, macrophages, and neutrophils in all three data sets after IS (Fig. 2F–H). Disease-free survival analysis showed that lower Ftl1 and Fth1 levels were associated with longer lifespan (Fig. 2I).

3.3. Elevated Ftl1 and Fth1 altered the function and cellular status of microglia, macrophages, and neutrophils

To systematically elucidate the effects of Ftl1 and Fth1 on the function and status of microglia, macrophages, and neutrophils, we

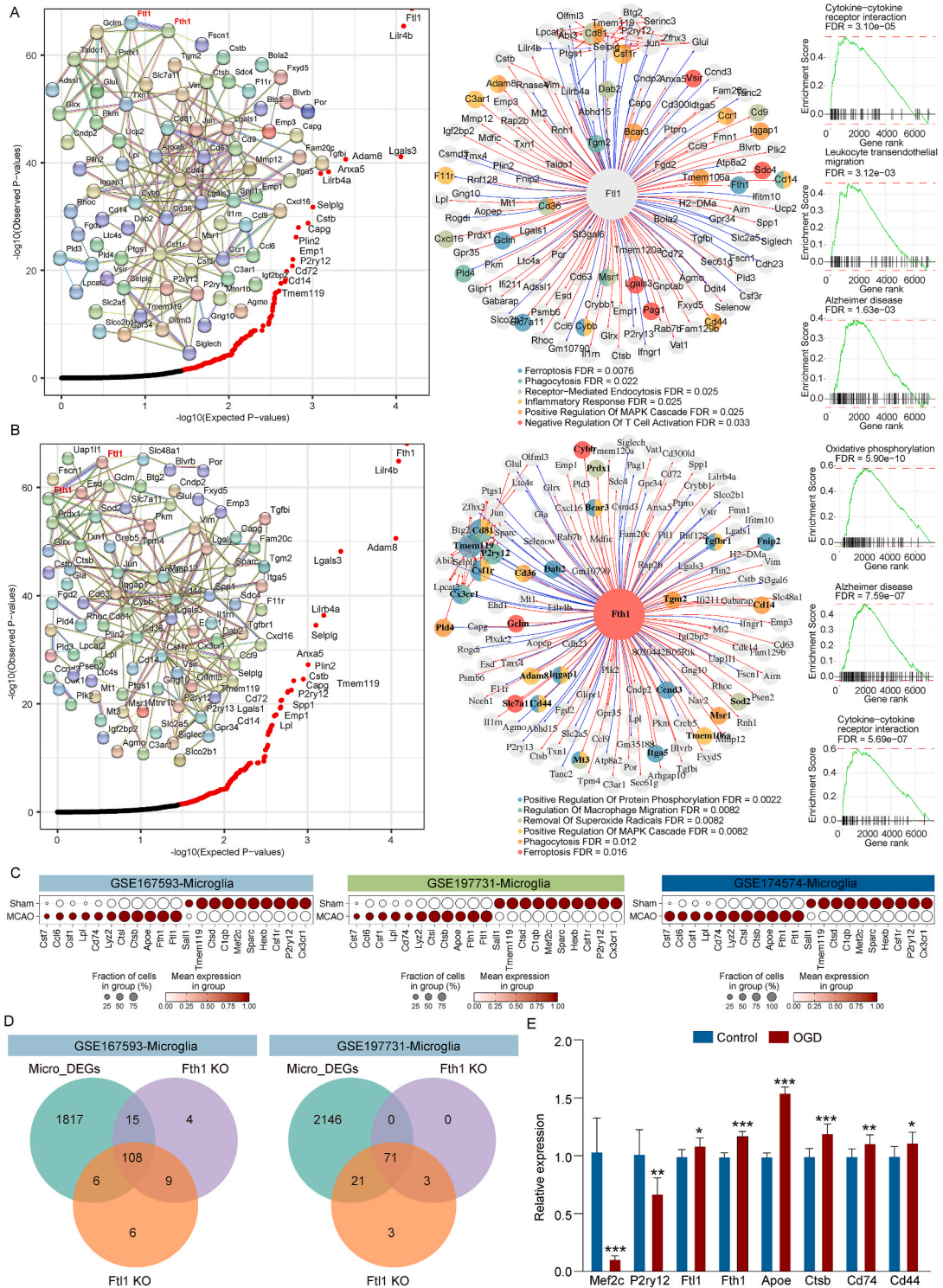


Fig. 3. Effects of *Ftl1* and *Fth1* KO on microglia transcriptome and function. **A.** Virtual KO of *Ftl1* in MCAO micro identifies gene expression program changes associated with *Ftl1*. QQ-plot of genes and interconnection of virtual KO perturbed genes in STRING are given (left). The egocentric plot (middle) shows the connections between the KO gene (*Ftl1*) and significant virtual KO perturbed genes (FDR < 0.05). Nodes are color-coded by each gene's membership association with enriched functional groups, as reported in the Enrichr analysis. The displaying gene sets are selected—only those with functions related to the Mendelian disease phenotype are shown. GSEA analysis identifies significant gene sets (right). **B.** Virtual KO of *Fth1* in MCAO micro identifies gene expression program changes associated with *Fth1*. QQ-plot of genes and interconnection of virtual KO perturbed genes in STRING are given (left). The egocentric plot (middle) shows the connections between the KO gene (*Fth1*) and significant virtual KO perturbed genes (FDR < 0.05). Nodes are color-coded by each gene's membership association with enriched functional groups, as reported in the Enrichr analysis. The displaying gene sets are selected—only those with functions related to the Mendelian disease phenotype are shown. GSEA analysis identifies significant gene sets (right). **C.** GSEA analysis identifies significant gene sets in Sham and MCAO groups for *Ftl1* and *Fth1*. **D.** Venn diagrams showing differentially expressed genes (DEGs) in *Ftl1* KO and *Fth1* KO groups. **E.** Bar graphs showing relative expression of selected genes in Control and OGD groups.

significant virtual KO perturbed genes (FDR <0.05). GSEA analysis identifies significant gene sets (right). C. Dotplot shows the expression of microglia homeostasis related genes and activation related genes in Sham and MCAO groups. D. Venn plots show the amount of overlap among Ftl1 and Fth1 KO perturbation genes and microglia DEGs. (For interpretation of the references to color in this figure legend, the reader is referred to the Web version of this article.)

applied scTenifoldKnk, a highly efficient virtual KO tool that allows individual systematic KO of multiple genes [30]. First, to investigate the molecular and cellular changes caused by Ftl1 and Fth1 KO in microglia, we extracted the snRNA-seq data of microglia in each of the three datasets and used the gene-cell expression matrix of MCAO samples as input to scTenifoldKnk (Fig. 3). In the GSE167593 dataset, the final scTenifoldKnk analysis report contained 129 and 135 significant genes affected by Ftl1 and Fth1 (FDR <0.05), respectively (Supplementary Table 3). These virtual KO perturbation genes included microglia marker genes P2ry12, Cx3cr1, and Csf1r (Fig. 3A and B). Based on the interaction enrichment analysis of the significant genes in the STRING protein-protein interaction database [36], we found that these genes were significantly connected in the interaction network ($p < 0.01$), indicating the close functional relationship among these genes (Fig. 3A and B). Functional enrichment analysis revealed that the disturbance gene of Ftl1 KO enrichment in ferroptosis, phagocytosis, receptor mediated endocytosis, inflammatory response, positive regulation of MAPK cascade (Fig. 3A). The disturbance gene of Fth1 KO enriched in positive regulation of protein phosphorylation, regulation of macrophage migration, and removal of superoxide radicals, positive regulation of MAPK cascade, phagocytosis, and ferroptosis (Fig. 3B). Subsequently, we performed gene set enrichment analysis (GSEA) analysis to assess the degree of disruption caused by Ftl1/Fth1 KO at the transcriptome level. GSEA analysis revealed that Ftl1/Fth1 KO affected functional genes related to Alzheimer's disease (AD), Parkinson's disease (PD), Huntington's disease (HD), oxidative phosphorylation, cytokine receptor interaction, and ferroptosis (Fig. 3B). The enrichment of AD, PD, and HD reflects the possibility that cerebral ischemic injury increases the prevalence of dementia.

In addition, we found that Fth1 KO significantly affected microglia homeostasis related genes such as P2ry12, Cx3cr, Csf1r, Hexb, Sparc, Mef2c, C1qb, Ctsd, Tmem 119, Sall1 and disease-related microglia marker genes, including Apoe, Ctsb, Ctsl, Lyz 2, Cd74, Lpl, Csf1, Ccl6, and Cst7 [37] (Fig. 3; Supplementary Table 3). The expression of Ftl1 and Fth1 in MCAO showed a positive correlation with disease-related microglia marker genes, but a negative correlation with microglia homeostasis related genes (Fig. 3C). Similar results were found in GSE197731 (Extended data Fig. 1; Supplementary Table 4). Most of these perturbed genes were included in the differential genes between Sham and MCAO (Fig. 3D). Similarly, we performed virtual KO of Ftl1 and Fth1 in macrophages (Extended data Fig. 2A and B; Extended data Fig. 3A and B) and neutrophils (Extended data Fig. 2C and D; Extended data Fig. 3C and D) for each of the three data sets. The results showed that in addition to GSE174574 dataset, both Ftl1 and Fth1 KO significantly affected genes related to inflammatory response activation, leukocyte migration and aggregation, neutrophil chemotaxis, and ferroptosis in macrophages and neutrophils in the other two datasets (Extended data Figs. 2 and 3; Supplementary Tables 5–8). Moreover, we found substantial overlap between Ftl1 and Fth1 perturbation genes and differential genes. These results indicate that Ftl1 and Fth1 are involved in the state and functional transition of microglia, macrophages, and neutrophils after ischemic brain injury in mouse, and significantly increase inflammatory response activation, migration, and aggregation of a variety of leukocytes. To verify the transcriptome changes of microglia after IS, we cultured BV2 microglia and constructed an OGD model. RT-qPCR showed that P2ry12 and Mef2c were significantly decreased in OGD group, while Ftl1, Fth1, Apoe, Ctsb, Cd44 and Cd74 were significantly increased in OGD group (Fig. 3E). In short, targeted therapy of Ftl1 and Fth1 in microglia may improve the state of microglia and tissue inflammatory response, thereby improving ischemic brain injury in mouse.

3.4. Chemotaxis of microglia to peripheral immune cells

The above results suggest that activated microglia might activate peripheral immune cells and promote their migration. Therefore, to investigate the chemotaxis of microglia to peripheral immune cells and its changes in MCAO, we analyzed the cellular communication between microglia and peripheral immune cells using cellchat. We found that the number of cell communication was downregulated overall after MCAO (Fig. 4A). Subsequently, we focused on the cellular communication that exists between microglia and macrophages and neutrophils. The results showed that there was a potential ligand receptor cell communication between microglia and macrophages through Spp1-Cd44 or App-Cd74, with Spp1-Cd44 and App-Cd74 cell communication significantly increased in the MCAO group (Fig. 4B–D). Previous studies have shown that SPP1 can act as a signaling molecule to recruit or activate immune cells and promote luteolysis and tissue degradation [38]. Therefore, we suggested that on the basis of blood brain barrier (BBB) leakage caused by IS, Spp1 released by microglia can recruit immune cells such as macrophages to reach the injured area through Cd44 receptors and further cause inflammatory responses. In addition, microglial Ftl1 and Fth1 KO could significantly reduce the expression of Spp1 (Fig. 3A and B), suggesting the regulatory role of microglia in immune cell chemotaxis. Immunohistochemical staining of human cerebral cortex showed that CD44 and CD74 were widely expressed in brain endothelial cells and perivascular cells, which provided the basis for microglia chemotaxis after MCAO (Fig. 4E). These results indicated that targeted therapy against Ftl1 and Fth1 might ameliorate ischemic brain injury in mouse by improving the state of microglia and reducing peripheral immune cell infiltration and tissue inflammation.

4. Discussion

In recent years, researchers have made some progress in understanding and intervening in ferroptosis caused by IS. The use of iron

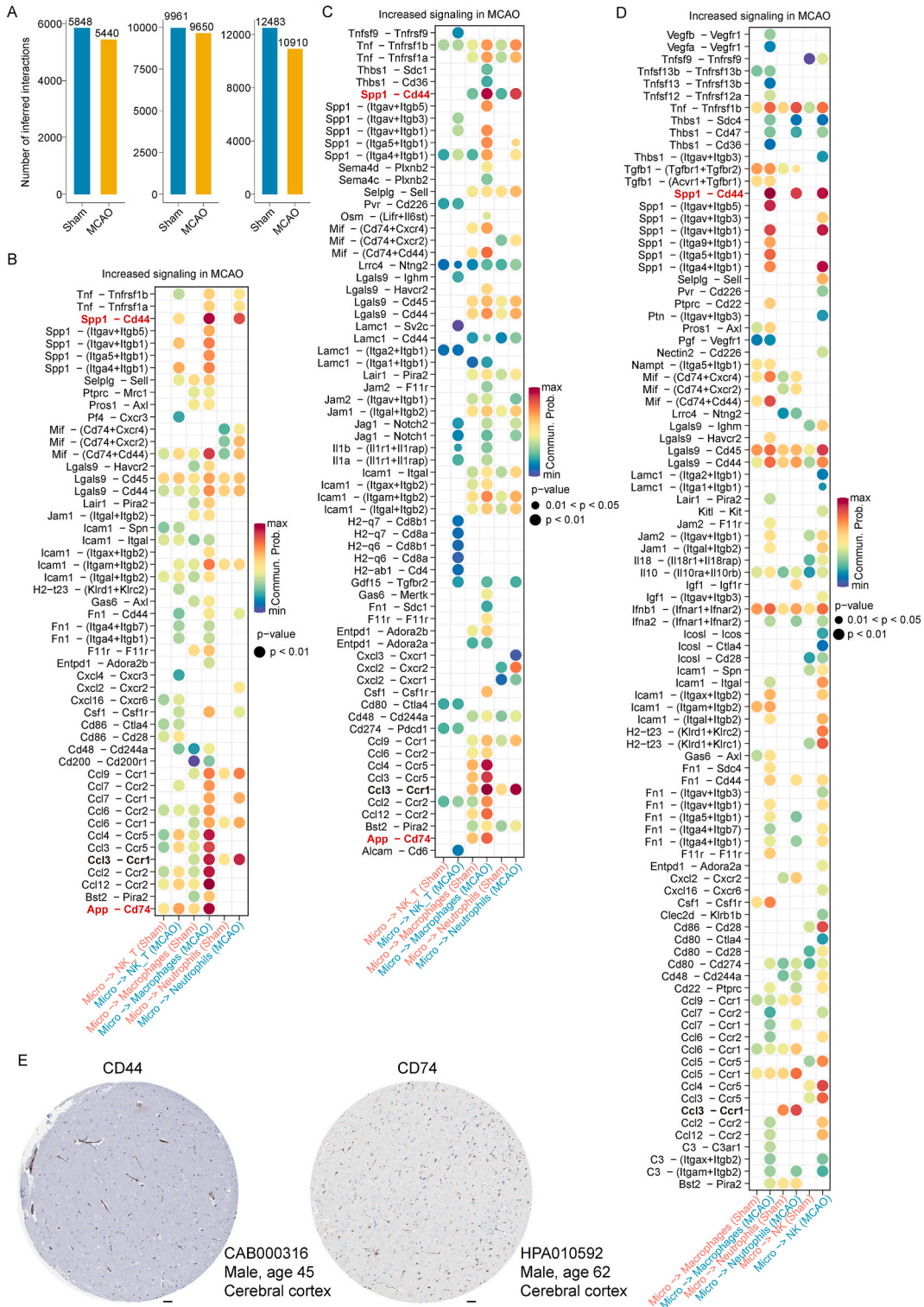


Fig. 4. Analysis of cell communication between Sham and MCAO groups. A. Bar graphs present the number of all cell communications in the sham and MCAO groups. B-D. Dotplot shows the cellular communication between microglia and macrophages and neutrophils in GSE167593 (B), GSE1997731 (C), and GSE174574 (D) datasets, respectively. Color coding represents the connection probability. E. IHC staining shows the expression of CD44 and CD74 in human cerebral cortex. Scale bars, 100 μ m. (For interpretation of the references to color in this figure legend, the reader is referred to the Web version of this article.)

chelators and antioxidants has a protective effect on reducing ferroptosis caused by IS. However, the role of microglial ferroptosis in cerebral ischemic injury has not been elucidated. In the present study, by analyzing snRNA-seq data from mouse IS, we found that the cell numbers of microglia, macrophages, and neutrophils were significantly upregulated after MCAO. Among the 12 PCD, ferroptosis was upregulated in most cell types after IS. Using machine learning, virtual gene KO, and cell communication analysis, we found that ferroptosis suppressor genes *Ftl1* and *Fth1* could promote microglia activation and the production of inflammatory factors and chemokines.

The concept of cell death used to be simple, with only two or three types, such as necrosis and apoptosis. Multiple modes of cell death have been progressively defined for more than a decade. In addition to the common forms of cell death, neurons also undergo several rare modes such as ferroptosis, pyroptosis and parthanatos [39]. Either mode of cell death is inextricable from the cascade of deleterious events that occur in IS. These deleterious pathological events influence each other and cross extensively in promoting cell death [40]. Previous studies have not compared the extent to which different modes of cell death are involved in different cells. Based on the snRNA-seq data, we clarified the differential and prevalent cell death in different cell types. Ferroptosis-related genetic alterations commonly occur in cell types after IS. Machine learning has also demonstrated the importance of ferroptosis in IS. Based on the feature importance ranking and gene KO, we found that ferroptosis suppressor genes *Fth1* and *Ftl1* could significantly affect the expression of microglia homeostasis genes and activation related genes. Studies have shown that *Fth1* and *Ftl1*, as ferroptosis inhibitory genes, can be significantly up-regulated by Cottonseed oil [41], Electroacupuncture [42], Quercetin [43], Insulin [44], and Ginkgolide B [45] to exert neuroprotective effects. This is questionable, because the elevation of *Fth1* and *Ftl1* is bound to aggravates the activation of microglia. It is well known that IS is more likely to occur in older individuals. Microglial activation also tends to occur in the aged brain [46] and may be associated with elevated *Fth1* and *Ftl1* [47,48]. The association of lower *FTL1* and *FTH1* levels with longer lifespan suggests a possible negative effect of elevated *Fth1* and *Ftl1*.

Previous studies have shown that neurons undergoing iron excess death release damage-associated molecular patterns (DAMPs) that can rapidly activate and recruit microglia, inducing upregulation of NADPH oxidase and production of ROS [16]. ROS can also act as proinflammatory signaling molecules and contribute to the activation of microglia [17]. Hyperactivated microglia secrete proinflammatory cytokines and chemokines that attract astrocytes and peripheral leukocytes, exacerbating neuroinflammation and oxidative stress [18]. Ultimately, a vicious cycle of mutual promotion and self-amplification between oxidative stress, neuronal ferroptosis, and inflammatory responses is formed, resulting in an injurious microenvironment detrimental to neural survival [24]. However, we found significant upregulation of ferroptosis-related genes in microglia itself. Among them, *Fth1* and *Ftl1* can promote the transition of microglia from the steady state to the activated state. Activated microglia possess a transcriptome profile similar to that of disease-associated microglia (DAMs) [37]. These activated microglia have a strong phagocytic capacity and tend to produce more inflammatory cytokines and chemokines.

Recently researches shown that T cells can infiltrate the brain in the context of neurodegenerative diseases [49,50] and during ageing [51]. Studies have shown that in AD mouse brain tissue, T cells actively interact with DAMs subsets. The depletion of microglia largely eliminated the infiltration of T cells, and the depletion of T cells also significantly hindered the activation of microglia, demonstrating the communication between the innate and adaptive immune cell families [49]. Aging is an important factor affecting BBB integrity. Studies have shown that age-related physiological or pathological changes in the composition of BBB cells can increase BBB's susceptibility to IS injury and lead to worsening brain damage [52]. On the basis of BBB disruption and high levels of chemokines in IS brain, activated microglia attract peripheral leukocytes to infiltrate the injury site in a concentration-dependent manner by means of specific ligand-receptor junctions (*Spp1*-*Cd44* and *App*-*Cd74*). Ferroptosis-related genes were also significantly upregulated in these leukocytes. Storm centers formed by these responses inhibit neuronal survival and synapse formation. The high expression of *CD44* and *CD74* in endothelial cells and perivascular leukocytes in human cerebral cortex suggested that these phenomena are not limited to mouse IS. Therefore, specifically transforming the expression of ferroptosis-related genes in microglia is expected to alleviate cerebral ischemic injury and improve the prognosis of patients.

In conclusion, our findings lay the foundation for implementing pleiotropic therapies to reshape the complex microenvironment for the treatment of IS. Nevertheless, this study also faces limitations. First, the study also requires additional protein analysis and functional validation to determine the role of microglial iron metabolism disorders in the progression of IS. Second, we cannot rule out the possibility that some cells or cell types are lost in the process of tissue separation, especially neutrophils, which contain low mRNA content and are only detectable in a very limited range. Third, we cannot completely rule out the effect of batch processing between datasets or the effect of sorting depth during data consolidation. Fourth, the chemotactic effect of microglia on other immune cells still needs a lot of basic experiments to verify. Despite all this, the improvement of iron metabolism disorder in microglia is potentially expected to be a key approach to the treatment of IS.

Funding

This study was supported by Yunnan Revitalization Talent Support Program (XDYC-MY-2022-0033), Foreign cooperation project of the Second Affiliated Hospital of Kunming Medical University (NO.2022dwhz18), and Social Development Specialized Project of Yunnan Provincial Key Technology Research and Development Program (No. 202203AC100007).

Data availability statement

All data associated with this study are present in the paper or the Supplementary Materials. The publicly available snRNA-seq datasets can be found in the Gene Expression Omnibus (GEO) under the accession number GSE167593, GSE1997731, and

GSE174574. The processed expression matrices used and/or analyzed during the current study have been deposited in the figshare (<https://figshare.com/>), under <https://doi.org/10.6084/m9.figshare.25815766>.

CRedit authorship contribution statement

Cheng-Long Shi: Writing – original draft, Data curation. **Xiu-Li Han:** Visualization. **Jing-Ce Chen:** Data curation. **Qian-Fan Pan:** Methodology. **Yong-Chao Gao:** Writing – original draft. **Peng-Yan Guo:** Data curation. **Xiao-Li Min:** Writing – review & editing. **Yong-Jun Gao:** Writing – review & editing, Conceptualization.

Declaration of competing interest

The authors declare that they have no conflict of interest.

Appendix A. Supplementary data

Supplementary data to this article can be found online at <https://doi.org/10.1016/j.heliyon.2024.e32727>.

References

- [1] X. Huo, et al., Trial of endovascular therapy for acute ischemic stroke with large infarct, *N. Engl. J. Med.* 388 (14) (2023) 1272–1283.
- [2] K. Walter, What is acute ischemic stroke? *JAMA* 327 (9) (2022) 885.
- [3] J. Bernhardt, et al., Stroke rehabilitation in low-income and middle-income countries: a call to action, *Lancet* 396 (10260) (2020) 1452–1462.
- [4] G.J. Hankey, Stroke, *Lancet* 389 (10069) (2017) 641–654.
- [5] Q.Z. Tuo, S.T. Zhang, P. Lei, Mechanisms of neuronal cell death in ischemic stroke and their therapeutic implications, *Med. Res. Rev.* 42 (1) (2022) 259–305.
- [6] R.B. Dietrich, W.G. Bradley Jr., Iron accumulation in the basal ganglia following severe ischemic-anoxic insults in children, *Radiology* 168 (1) (1988) 203–206.
- [7] S.J. Dixon, et al., Ferroptosis: an iron-dependent form of nonapoptotic cell death, *Cell* 149 (5) (2012) 1060–1072.
- [8] S. Ahmad, et al., Sesamin attenuates neurotoxicity in mouse model of ischemic brain stroke, *Neurotoxicology* 45 (2014) 100–110.
- [9] I. Alim, et al., Selenium drives a transcriptional adaptive program to block ferroptosis and treat stroke, *Cell* 177 (5) (2019) 1262–1279.e25.
- [10] L.E. Pope, S.J. Dixon, Regulation of ferroptosis by lipid metabolism, *Trends Cell Biol.* 33 (12) (2023) 1077–1087.
- [11] Q.Z. Tuo, et al., Tau-mediated iron export prevents ferroptotic damage after ischemic stroke, *Mol Psychiatry* 22 (11) (2017) 1520–1530.
- [12] R. Kang, et al., Lipid peroxidation drives gasdermin D-mediated pyroptosis in lethal polymicrobial sepsis, *Cell Host Microbe* 24 (1) (2018) 97–108.e4.
- [13] W.S. Yang, et al., Regulation of ferroptotic cancer cell death by GPX4, *Cell* 156 (1–2) (2014) 317–331.
- [14] L. Chen, et al., Ablation of the ferroptosis inhibitor glutathione peroxidase 4 in neurons results in rapid motor neuron degeneration and paralysis, *J. Biol. Chem.* 290 (47) (2015) 28097–28106.
- [15] X. Guan, et al., The neuroprotective effects of carvacrol on ischemia/reperfusion-induced hippocampal neuronal impairment by ferroptosis mitigation, *Life Sci.* 235 (2019) 116795.
- [16] E. Gülke, M. Gelderblom, T. Magnus, Danger signals in stroke and their role on microglia activation after ischemia, *Ther Adv Neurol Disord* 11 (2018), 1756286418774254.
- [17] M.A. Yenari, T.M. Kauppinen, R.A. Swanson, Microglial activation in stroke: therapeutic targets, *Neurotherapeutics* 7 (4) (2010) 378–391.
- [18] S. Dabrowska, et al., Neuroinflammation as a target for treatment of stroke using mesenchymal stem cells and extracellular vesicles, *J. Neuroinflammation* 16 (1) (2019) 178.
- [19] Y. Yu, et al., Ferroptosis: a cell death connecting oxidative stress, inflammation and cardiovascular diseases, *Cell Death Dis.* 7 (1) (2021) 193.
- [20] S.K. Ryan, et al., Microglia ferroptosis is regulated by SEC24B and contributes to neurodegeneration, *Nat. Neurosci.* 26 (1) (2023) 12–26.
- [21] S. Liu, X. Gao, S. Zhou, New target for prevention and treatment of neuroinflammation: microglia iron accumulation and ferroptosis, *ASN Neuro* 14 (2022), 17590914221133236.
- [22] Y. Cui, et al., Microglia and macrophage exhibit attenuated inflammatory response and ferroptosis resistance after RSL3 stimulation via increasing Nrf2 expression, *J. Neuroinflammation* 18 (1) (2021) 249.
- [23] Y. Jin, et al., Inhibiting ferroptosis: a novel approach for stroke therapeutics, *Drug Discov. Today* 26 (4) (2021) 916–930.
- [24] A. Drieu, et al., Anti-inflammatory treatments for stroke: from bench to bedside, *Ther Adv Neurol Disord* 11 (2018), 1756286418789854.
- [25] S.F. Lau, et al., Single-nucleus transcriptome analysis reveals dysregulation of angiogenic endothelial cells and neuroprotective glia in Alzheimer's disease, *Proc Natl Acad Sci U S A* 117 (41) (2020) 25800–25809.
- [26] X. Fan, et al., Single-cell transcriptome analysis reveals cell lineage specification in temporal-spatial patterns in human cortical development, *Sci. Adv.* 6 (34) (2020) eaaz2978.
- [27] R.Z. Niu, et al., Integrated analysis of plasma proteome and cortex single-cell transcriptome reveals the novel biomarkers during cortical aging, *Front. Aging Neurosci.* 15 (2023) 1063861.
- [28] T. Stuart, et al., Comprehensive integration of single-cell data, *Cell* 177 (7) (2019) 1888–1902.e21.
- [29] L. Schirmer, et al., Neuronal vulnerability and multilineage diversity in multiple sclerosis, *Nature* 573 (7772) (2019) 75–82.
- [30] D. Osorio, et al., scTenifoldKnk: an efficient virtual knockout tool for gene function predictions via single-cell gene regulatory network perturbation, *Patterns (N Y)* 3 (3) (2022) 100434.
- [31] X. Shi, et al., Stroke subtype-dependent synapse elimination by reactive gliosis in mice, *Nat. Commun.* 12 (1) (2021) 6943.
- [32] S. Kim, et al., The antioxidant enzyme Peroxiredoxin-1 controls stroke-associated microglia against acute ischemic stroke, *Redox Biol.* 54 (2022) 102347.
- [33] K. Zheng, et al., Single-cell RNA-seq reveals the transcriptional landscape in ischemic stroke, *J Cereb Blood Flow Metab* 42 (1) (2022) 56–73.
- [34] E. Dann, et al., Differential abundance testing on single-cell data using k-nearest neighbor graphs, *Nat. Biotechnol.* 40 (2) (2022) 245–253.
- [35] Y. Zou, et al., Leveraging diverse cell-death patterns to predict the prognosis and drug sensitivity of triple-negative breast cancer patients after surgery, *Int. J. Surg.* 107 (2022) 106936.
- [36] J. Jia, et al., Stress granules and mTOR are regulated by membrane atg8ylation during lysosomal damage, *J. Cell Biol.* 221 (11) (2022).
- [37] H. Keren-Shaul, et al., A unique microglia type associated with restricting development of Alzheimer's disease, *Cell* 169 (7) (2017) 1276–1290.e17.
- [38] P.O. Azevedo, et al., Endothelial cells maintain neural stem cells quiescent in their niche, *Neuroscience* 363 (2017) 62–65.
- [39] M. Fricker, et al., Neuronal cell death, *Physiol. Rev.* 98 (2) (2018) 813–880.
- [40] R. Mao, et al., Neuronal death mechanisms and therapeutic strategy in ischemic stroke, *Neurosci. Bull.* 38 (10) (2022) 1229–1247.
- [41] M. Sun, et al., Cottonseed oil alleviates ischemic stroke injury by inhibiting ferroptosis, *Brain Behav* 13 (10) (2023) e3179.

- [42] G. Li, et al., Electroacupuncture ameliorates cerebral ischemic injury by inhibiting ferroptosis, *Front. Neurol.* 12 (2021) 619043.
- [43] C. Peng, et al., Quercetin attenuates cerebral ischemic injury by inhibiting ferroptosis via Nrf2/HO-1 signaling pathway, *Eur. J. Pharmacol.* 963 (2024) 176264.
- [44] M. Sun, et al., Insulin alleviates lipopolysaccharide-induced cognitive impairment via inhibiting neuroinflammation and ferroptosis, *Eur. J. Pharmacol.* 955 (2023) 175929.
- [45] Y. Yang, et al., Ginkgolide B attenuates IS-reperfusion injury via inhibition of ferroptosis through disrupting NCOA4-FTH1 interaction, *J. Ethnopharmacol.* 318 (Pt B) (2024) 116982.
- [46] A. Silvin, et al., Dual ontogeny of disease-associated microglia and disease inflammatory macrophages in aging and neurodegeneration, *Immunity* 55 (8) (2022) 1448–1465.e6.
- [47] R. Tortuyaux, et al., Physiopathological changes of ferritin mRNA density and distribution in hippocampal astrocytes in the mouse brain, *J. Neurochem.* 164 (6) (2023) 847–857.
- [48] A. Datta, et al., Novel pathophysiological markers are revealed by iTRAQ-based quantitative clinical proteomics approach in vascular dementia, *J. Proteomics* 99 (100) (2014) 54–67.
- [49] X. Chen, et al., Microglia-mediated T cell infiltration drives neurodegeneration in tauopathy, *Nature* 615 (7953) (2023) 668–677.
- [50] D. Sulzer, et al., T cells from patients with Parkinson's disease recognize α -synuclein peptides, *Nature* 546 (7660) (2017) 656–661.
- [51] B.W. Dulken, et al., Single-cell analysis reveals T cell infiltration in old neurogenic niches, *Nature* 571 (7764) (2019) 205–210.
- [52] W. Cai, et al., Dysfunction of the neurovascular unit in ischemic stroke and neurodegenerative diseases: an aging effect, *Ageing Res. Rev.* 34 (2017) 77–87.